*Desalination and Water Treatment*
www.deswater.com

doi: 10.5004/dwt.2020.25690

193 (2020) 142–151
July

# Adsorptive removal of Methyl orange from aqueous solutions by polyvinylidene fluoride tri-flouro ethylene/carbon nanotube/kaolin nanocomposite: kinetics, isotherm, and thermodynamics

M. El Gamal[a], F.M. Mohamed[b,*], M.A. Mekewi[c], F.S. Hashem[c], M.R. El-Aassar[d,e], R.E. Khalifa[e]

[a]*Science and technology center of excellence (STCE), National Organization for Military Production, Egypt*
[b]*Faculty of Earth Sciences, Beni-Suef University, P.O. 62521, Beni-Suef, Egypt, emails: fathy19730306@gmail.com/fathy1973@esc.bsu.edu.eg (F.M. Mohamed)*
[c]*Chemistry Department, Faculty of Science, Ain Shams University, P.O. Box: 11566, Cairo, Egypt*
[d]*Department of Chemistry, College of Science, Jouf University, Sakaka 2014, Saudi Arabia*
[e]*Polymer Materials Research Department, Advanced Technology and New Material Institute, City of Scientific Research and Technological Applications (SRTA City), New Borg El-Arab City, P.O. Box: 21934, Alexandria, Egypt*

Received 6 December 2019; Accepted 12 February 2020

**ABSTRACT**

In the present study, the poly(vinylidene fluoride–trifluoroethylene), P(VDF–TrFE)/non functionalized multi-walled carbon nanotubes (MWCNTs)/kaolin composite, (P(VDF–TrFE)/MWCNTs/K) was prepared successfully for the removal of Methyl orange from aqueous solutions with high adsorption capacity. The physicochemical properties were characterized via Fourier transform infrared spectroscopy, X-ray diffraction, and thermogravimetric analysis. Batch adsorption experiments were conducted to evaluate the influence of contact time, pH, adsorbent dose, agitation rate, initial dye concentration, and temperature. The experimental equilibrium adsorption data indicate that the monolayer coverage is 62.89 mg/g. The recyclability and regeneration of the composite were investigated and illustrated that the composite could be recycled at least three times. Adsorption kinetics and thermodynamics were also studied. Therefore, the developed composite is regarded as a better adsorbent to address industrial wastewater in Egypt with low-cost and excellent efficiency.

*Keywords:* Poly(vinylidene fluoride–trifluoroethylene); MWCNTs; Kaolin; Composite; Methyl orange removal; Adsorption, Kinetics; Thermodynamics

## 1. Introduction

Dyestuffs are excessively utilized in industries like tissues, pulp mills, newspapers, dyestuff synthesis, foodstuff, publishing, leather tanning, rubber, pharmacy, drugs, cosmetics, chemical labs, and plastics industries. For the time being, several types of azo-organic dyes are used in leather, electroplating, textile, paper-manufacturing, plastics, and printing manufactures [1–3].

Each industry emits a huge quantity of dye-containing wastewater that has a toxic outcome for human health [3–5]. Besides, contamination from dye wastewater is becoming a severe environmental problem. Thus, removal of color from wastewater is very stringent for treating the fundamental environmental, biological, and industrial problems accompanying the dyes and stains [6].

Improving an efficacious method for the administration and optimization of the dyestuff industry has long been the main target for environmental protection. Several techniques, including chemical oxidation, ozonation, photochemical degradation with a metal oxide such as zinc oxide and titanium oxide, membrane separation, coagulation/flocculation,

* Corresponding author.

*Presented at the 4th International Water Desalination Conference: Future of Water Desalination in Egypt and the Middle East, 24–27 February 2020, Cairo, Egypt*

and adsorption, were employed to eliminate dyes from wastewaters [7]. Adsorption is one of the most effective methods that have been used successfully in this field [8–13].

Multi-wall carbon nanotubes (MWCNTs) and single-wall carbon nanotubes have large specific surface areas and have found utility as adsorbents for both aqueous organic and inorganic contaminants, many researchers have been used carbon nanotubes (CNs) in wastewater treatment especially organic materials [14–21].

Chemisorption or physical sorption of colored compounds from aqueous solution has predicted in a superior way to treat effluent with low-cost [22–24].

Methyl orange (MO) is a kind of the p-aminoazobenzene (p-AAB) dyes. It is easily utilized in the textile stain industry and chemical experiments as well as an acid-base indicator in research laboratories and labs. However, the aqueous solution of MO is toxic and irritating. Thus, removal of MO from aqueous solution is of great weight and accomplished via different techniques [25–32].

The present work explored the utilization of poly (vinylidene fluoride–trifluoroethylene P(VDF–TrFE)/CN/kaolin for MO removal from aqueous medium. The adsorption experiments were conducted using a batch adsorption system, it was enhanced by applying the influence of important affecting factors such as (pH, amount of adsorbent, initial MO concentration, agitation speed, and contact time). The precursors and composite were been characterized by different analytical techniques such as XRF, X-ray diffraction (XRD), IR, and thermogravimetric analysis (TGA). In addition, the adsorption kinetics, isotherm, and thermodynamics were also investigated.

## 2. Materials and methods

### 2.1. Chemicals

Methyl orange dye (MO), (4-[[(4-Dimethylamino) phenyl] azo] benzene sulfonic acid sodium salt, C.I. 13025, MW = 327.34 g/mole, dye content 85%) was bought from Fluka, Switzerland laboratory grade. $H_2SO_4$ and NaOH were supplied from Al-Ghomhoria Company.

Non functionalized multi-walled carbon nanotubes (MWCNT's; purity > 95%, nominal outside diameter = 40–50 nm and length = 5–15 μm) was brought from science and technology center of excellence (STCE), National Authority for Military Production. P(VDF–TrFE) containing 30% wt. TrFE was purchased from Piezotech in France. N,N-Dimethyl formamide (DMF) was obtained from Sigma-Aldrich. Natural kaolin was collected from Egypt desert.

### 2.2. Preparation of P(VDF–TrFE)/MWCNT/K nanocomposite

0.25 g MWCNT's and 10 g kaolin were ultrasonically dispersed in DMF at room temperature for 2 h to form a stable suspension. Two precautions were taken to prevent breaking of the nanotubes; the first one, set the probe to work with only 50% of maximum amplitude and the second one was to set it to work in pulses. At the same time, 0.5 g P(VDF-TrFE) copolymer was dissolved in DMF. Then the suspension of MWCNT's in DMF was added to the P(VDF-TrFE) solution, the mixture was magnetically stirred for 30 min at the UP 200S ultrasonic lab device (200 W–24 KHz) used as a powerful homogenizer, deagglomeration and dispersion, supplied by Hielscher ultrasonics GmbH company (Germany). The mixture was then subjected to an ultrasonic treatment for another 30 min. The final nanocomposite solutions were cast in a 50 ml petri dish, degassed in a vacuum oven, and kept in a hood for a period of 24 h for the solvent evaporation. The nanocomposite was dried at room temperature, peeled off from the petri dish, and annealed at 90°C for 6 h, then the dried nanocomposite was ground well by using a ceramic mortar and pistol.

### 2.3. Batch adsorption experimental analysis

A certain weight of P(VDF–TrFE)/MWCNT/K nanocomposite was weighed and mixed into100 mL of definite concentration of MO solution. Variation of the P(VDF–TrFE)/MWCNT/K dose 10–60 mg/L and initial dye concentration 25–150 mg/L at different agitation rates 50–25 rpm for 0–120 min using an orbital shaker (Yellow line, Germany) was studied. The MO solution was separated from the adsorbent by centrifugation at 12,000 rpm using a centrifuge, (Hettich, Model EBA 200, Germany), for 30 min. The MO concentrations in the supernatant were estimated using a single beam UV/Vis spectrophotometer (HACH DR 6000) at wavelength 468 nm according to [33]. Each sample was tested three times and the average result was recorded. Eqs. (1) and (2) were applied to estimate the removal percentage and the uptake capacity (mg/g), respectively, where $C_0$ (mg/L) is the initial concentration of MO and $C_e$ (mg/L) is the equilibrium concentration of MO in solution, $V$ is the volume in L and $W$ is the adsorbent mass (g).

$$\text{Removal}\% = \frac{C_0 - C_e}{C_e} \times 100 \tag{1}$$

$$q_e = \frac{\left(C_0 - C_e\right)V}{M} \tag{2}$$

### 2.4. Isothermal and kinetic investigation of MO onto P(VDF–TrFE)/MWCNT/K nanocomposite

Langmuir and Freundlich isotherms were applied to evaluate the MO adsorption mechanism onto the P(VDF–TrFE)/MWCNT/K adsorbent (Table 1). As well as kinetic sorption models, Lagergren's pseudo-first-order model [34], and pseudo-second-order model (Table 2).

### 2.5. Estimation of thermodynamic parameters

Thermodynamic parameters such as Gibb's free energy ($\Delta G$), enthalpy ($\Delta H$), and entropy ($\Delta S$) changes can be determined by the Eqs. (3)–(5) as follows [37]:

$$\Delta G = -RT \ln K_0 \tag{3}$$

$$\ln K_0 = -\frac{\Delta G}{RT} \tag{4}$$

Table 1
Adsorption isotherm models for MO uptake by P(VDF–TrFE)/MWCNT/K nanocomposite

| Isotherm model | Linear form | Parameters |
|---|---|---|
| Langmuir [35] | $\frac{C_e}{q_e}=\frac{1}{q_{max}b}+\frac{C_e}{q_{max}}$<br>$R_L = 1/(1 + bC_0)$<br>$R_L > 1$ (unfavorable adsorption)<br>$R_L = 1$ (linear adsorption)<br>$(0 < R_L < 1$ (favorable adsorption)<br>$R_L = 0$ (irreversible adsorption) | $C_e$ (mg/L): equilibrium concentration of the resting MO in the solution<br>$q_e$ (mg/g): removed amount of MO at equilibrium<br>$q_{max}$ (mg/g): maximum adsorption capacity<br>$b$ (L/mg): Langmuir constant<br>$q_{max}$ = 1/slope<br>$b$ = slope/intercept<br>$C_0$: initial MO concentration<br>$R_L$: equilibrium parameter of the Langmuir equation |
| Freundlich [36] | $\log q_e = \log K_F + \frac{1}{n}\log C_e$ | $C_e$ (mg/L): equilibrium concentration of the resting MO in the solution<br>$q_e$ (mg/g): removed amount of MO at equilibrium<br>$K_F$ (mg/g): MO adsorption capacity<br>$n$: heterogeneity factor<br>$K_F = 10^{intercept}$<br>$1/n$ = slope |

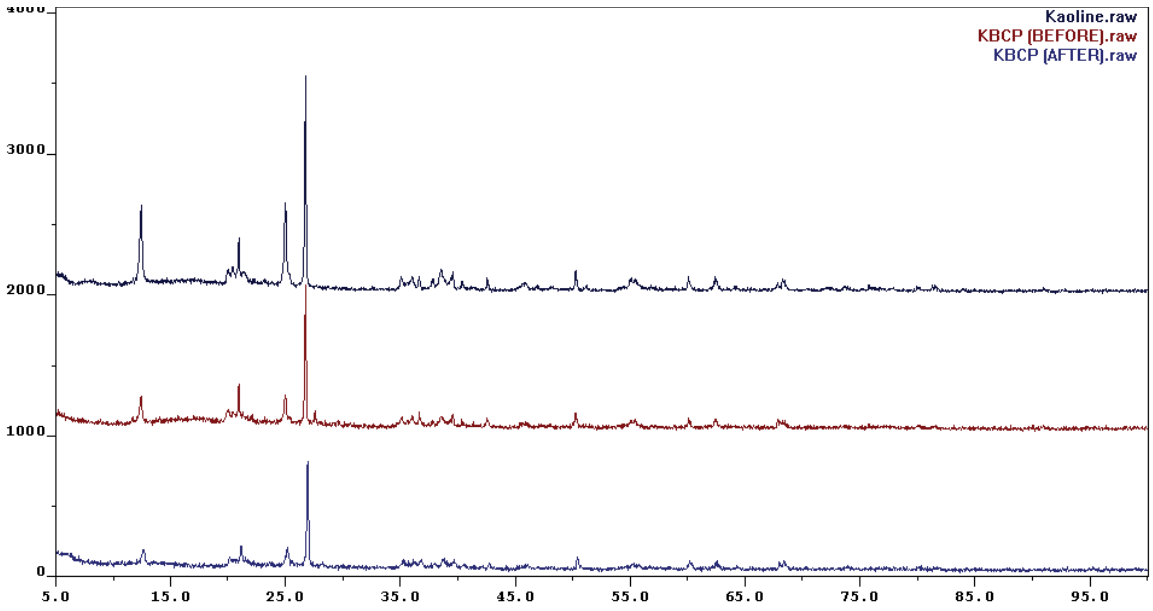


Fig. 1. XRD patterns for P(VDF–TrFE)/MWCNT/K nanocomposite before and after up taking.

$$\ln K_0 = -\frac{\Delta S}{R} - \frac{\Delta H}{RT} \quad (5)$$

where $R$ is the universal gas constant (8.314 J/mol/K) and $T$ is the absolute temperature in Kelvin.

## 3. Results and discussion

### 3.1. Characterization of kaolin, MWCNTs, and P(VDF–TrFE)/MWCNT/K

#### 3.1.1. X-Ray diffraction

The spectrum shows the kaolin is highly crystalline as the peaks are narrow. The main peaks that appeared at 2θ = 20.89° and 26.65° are characteristic bands for quartz $SiO_2$ which is a silica polymorph consisting of interconnected $SiO_2$ tetrahedral that build up a rigid three-dimensional network. The peak at 2θ = 12.41° and 50.13° are characteristic for the kaolinite clay mineral.

#### 3.1.2. Thermal characterization

The thermal stabilities of the nanocomposite were evaluated by TGA (TA Instruments Q500 equipment thermogravimetric analyzer). Samples were heated at nitrogen purge flow 50 mL/min at 25°C–900°C at a heating rate of 10°C/min. The glass transition of the polymer was further studied by differential scanning calorimetry (TA Instruments

Q2000 DSC). The thermal history of the samples was erased by heating from 25°C–350°C at a heating rate of 10°C/min and a nitrogen purge flow of 50 mL/min. These devices were available at STCE.

Fig. 2 illustrates the TGA curves of P(VDF–TrFE)/MWCNT/K nanocomposite. It can be seen that the sample has four degradation stages. The first stage starts at 108.64°C, which attributed to the loss of free moistures. The second stage is in the range of 255.84°C–546.19°C and mainly occurred due to the degradation of the polymeric main chain of P(VDF–TrFE). In this stage the decomposition temperature of P(VDF–TrFE) is 315°C (weight loss 16.84%). The third stage is over 546.19°C and is mainly due to the removal of organic carbon of P(VDF–TrFE). In the fourth stage the clay convert from amorphous to crystalline form. On the other hand, the degradation of P(VDF–TrFE) is one stage only at 546.19°C as shown in Fig. 3. Thus, it can be verified that the thermal stability of P(VDF–TrFE) is better than that of the P(VDF–TrFE)/MWCNT/K copolymer.

#### *3.1.3. Fourier transform infrared spectroscopy characterization*

The FTIR spectra of P(VDF–TrFE)/MWCNT/K were shown in Fig. 4a. The bands at 3,479.58 and 3,410.15 $cm^{-1}$ are assigned to the coupled OH stretching mode. These are the 2 coupled hydroxyl groups that are characteristic of the kaolinite clay minerals. The band at 3,410.15 $cm^{-1}$ lies wholly within the kaolin layers with the proton end directed towards the octahedral repeat layers. The other hydroxyl band at 3,479.58 $cm^{-1}$ is positioned in a way that allows hydrogen bonding to the oxygen from the adjacent repeat layer; also the dipoles of this hydroxyl group are perpendicular to the surface of the crystal, giving a negative overall charge of the surface of the clay. The Si–OH and Si–O– bending respectively are found at 1,033.26 and 1,005.17 $cm^{-1}$ respectively. The Al–Al–O deformation asymmetric stretch is found at band 918.12 $cm^{-1}$. The Al–O–Si inner vibration observed at 786.12 $cm^{-1}$ is due to the presence of quartz in the clay sample. This is also supported by the presence of the band at 694.37 $cm^{-1}$. The peaks appeared at 600, 745, and 840 $cm^{-1}$ ,as well as a peak at 2,816.93 $cm^{-1}$ are pointed to the bending and stretching of CH=CH of the vinylidene group of P(VDF–TrFE)/ [38]. The peaks at 1,805 $cm^{-1}$ and several peaks in the range of 3,000 $cm^{-1}$ range were attributed to CHx groups of MWCNTs [39]. The peaks at 3,447 $cm^{-1}$ may be associated with O–H and presented two dominant peaks; 1,600 and 3,450 $cm^{-1}$ [40].

Fig. 4b shows the FTIR spectra of P(VDF–TrFE)/MWCNT/K after up taking of MO, the main peaks of nanocomposite is present, and only shifted to lower wavenumber, the appearance of peak around 1,300 $cm^{-1}$ indicated the uptaking of MO. The appearance of a peak at 3,618 $cm^{-1}$ may be due to the NH group of MO. The presence of a peak at 3,232.1 $cm^{-1}$ may be a rearrangement of the methyl group in acidic media to giving a triple bond of C–C bonding.

The peak at 1,604 $cm^{-1}$ represented the C–N stretching that showed a lower wavenumber in comparison with the position before the adsorption process at 1,625 $cm^{-1}$. Further, the peak intensity of C–N at 1,604 $cm^{-1}$ is increased after the adsorption of MO dyes over P(VDF–TrFE)/MWCNT/K [41]. The band in the range of 1,350 $cm^{-1}$ is due to the stretching of –S=O group indicating successful adsorption of MO dye on the adsorbent surface. Moreover, the weak band at 1,033 $cm^{-1}$ corresponds to the –N=N– stretching vibration and shifted to low wave number 1,022 $cm^{-1}$ [42].

### *3.2. Factors affecting the adsorption process*

#### *3.2.1. Effect of pH*

The adsorption of MO by P(VDF–TrFE)/MWCNT/K nanocomposite is a pH-dependent process. The results indicated that the removal percent (*R*%) of MO was very high at low pH values as demonstrated in Fig. 5, and the

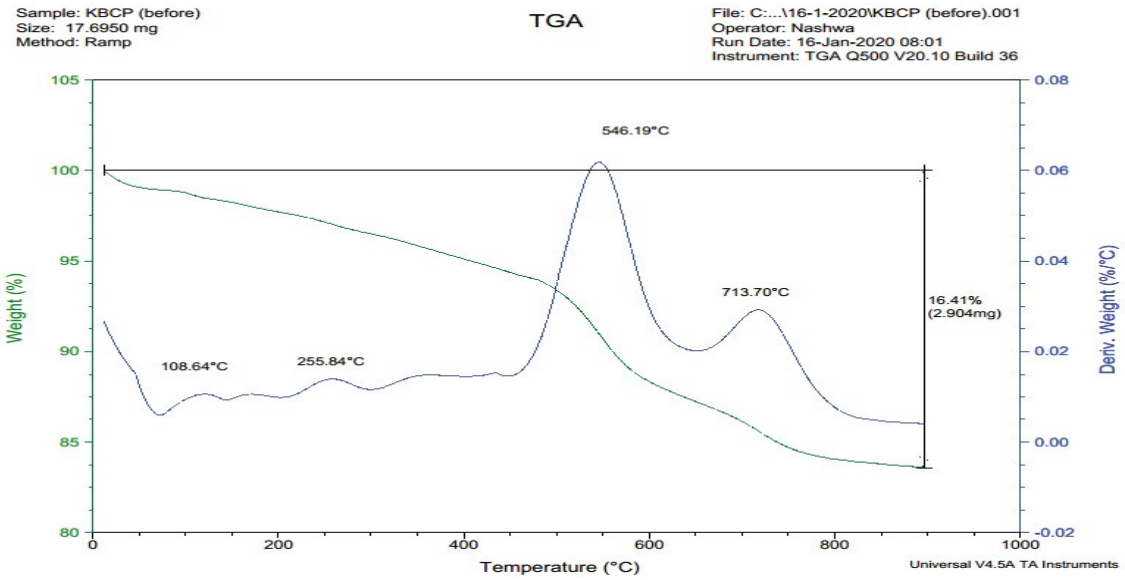


Fig. 2. TGA curve of P(VDF–TrFE)/MWCNT/K.

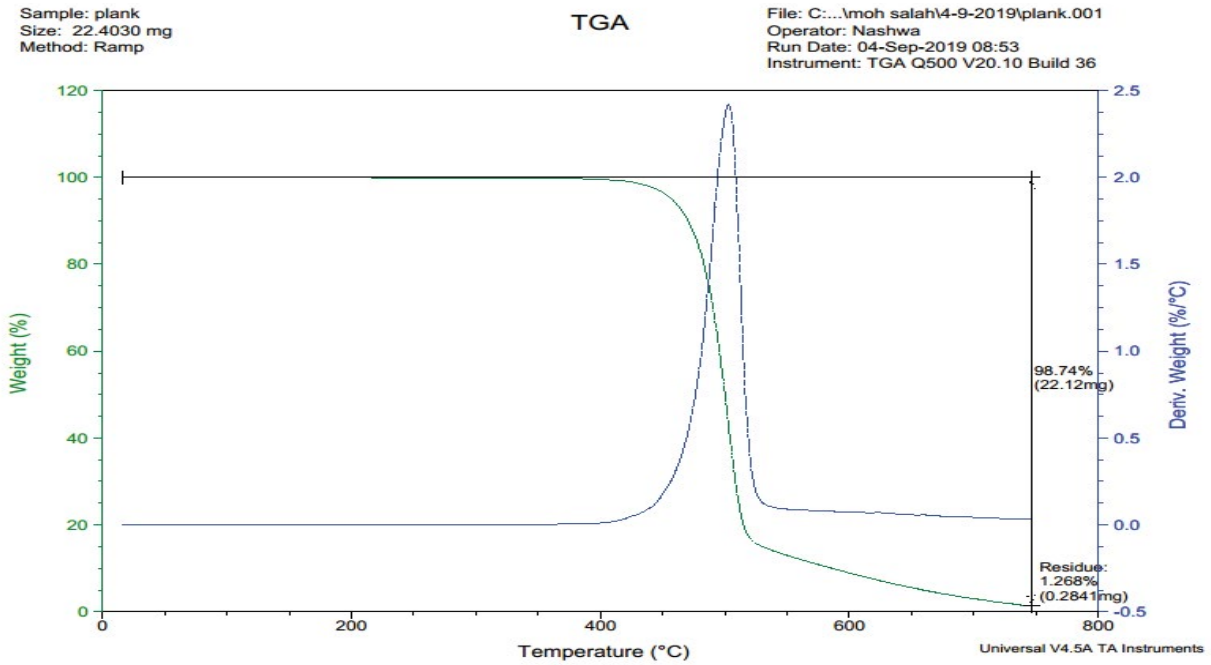


Fig. 3. TGA curve of P(VDF–TrFE).

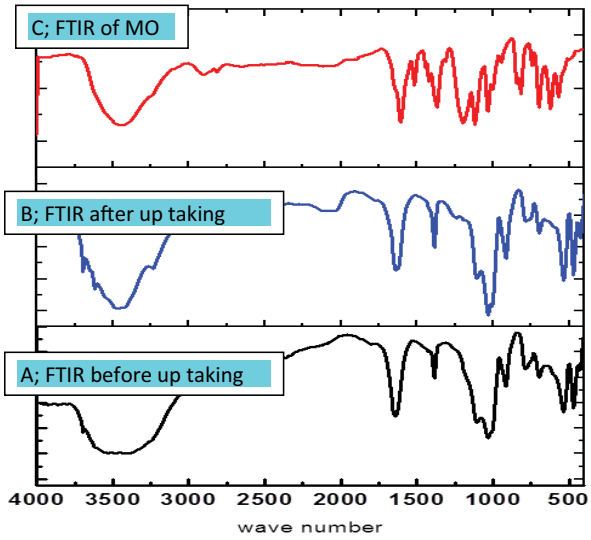


Fig. 4. FTIR spectra of P(VDF–TrFE)/MWCNT/K and MO.

maximum removal efficiency (92.9%) was achieved at pH 3.0. Therefore, the pH = 3 was selected as the optimum pH and applied for all the adsorption studies to verify equilibrium accomplishment.

### 3.3. Effect of contact time

The adsorption outline of MO by P(VDF–TrFE)/MWCNT/K nanocomposite at several selected times (5–100 min) is demonstrated in Fig. 6. The results revealed that adsorption was very rapid at the beginning (5–60 min) then reach equilibrium at 90 min. This behavior is because of the electrostatic interactions which facilitate the diffusion

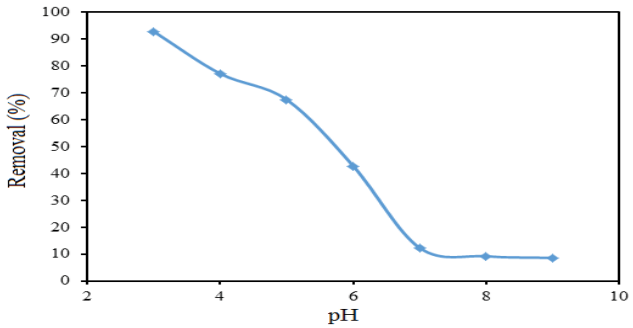


Fig. 5. Effect of pH on the adsorption of MO onto P(VDF–TrFE)/MWCNT/K nanocomposite.

of extra dye molecules to the interior free sites. Moreover, during the initial stage, a large number of vacant surface localities were available, while the remaining vacant surface sites after a lapse of time were difficulty packed attributable to the repellence forces amongst the dye molecules on the solid and bulk phases. In contrast, with increasing contact time beyond 90 min, the diffusion becomes more difficult as the vacant volume within the adsorbent decreases. Thus, the affinity of sorbent towards MO molecules decreased.

### 3.4. Effect of initial MO concentration

The adsorption of MO was conducted at different dye concentrations as shown in Fig. 7. The results showed that increasing the MO concentration cause a decrease in the removal percent from 96% to 59%. Therefore, aqueous dye solution with initial MO concentration = 100 mg/L was appropriated for all the adsorption studies to verify equilibrium accomplishment

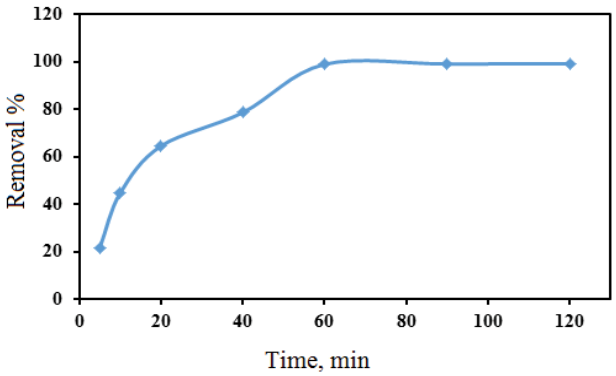


Fig. 6. Effect of time on the adsorption of MO onto P(VDF–TrFE)/MWCNT/K nanocomposite.

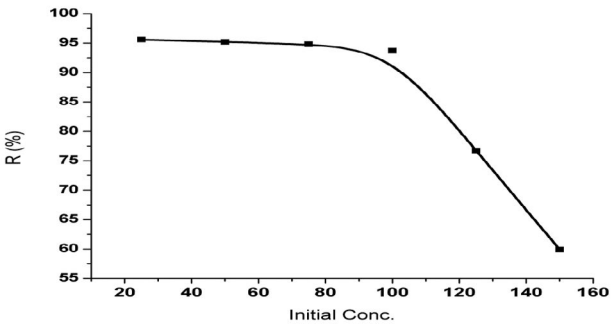


Fig. 7. Effect of initial MO concentration on the adsorption of MO onto P(VDF–TrFE)/MWCNT/K nanocomposite.

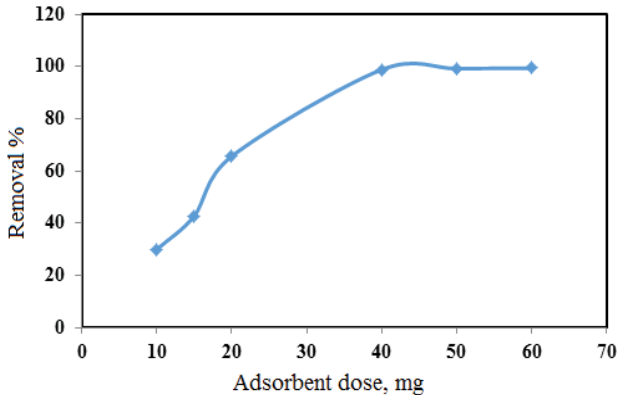


Fig. 8. Effect of adsorbent dose on the adsorption of MO onto P(VDF–TrFE)/MWCNT/K nanocomposite.

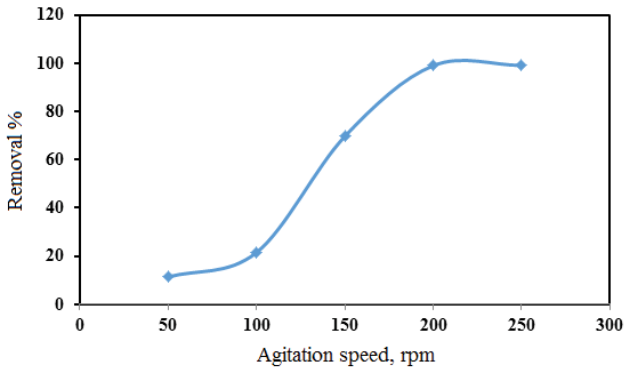


Fig. 9. Effect of adsorbent dose on the adsorption of MO onto P(VDF–TrFE)/MWCNT/K nanocomposite.

### 3.5. Effect of adsorbent mass

Indeed, the impact of the primary adsorbent dosage is an important feature in large scale applications. The consequence of the adsorbent amount on the removal % was studied (10–60 mg). It was obvious from Fig. 8 that increasing the P(VDF–TrFE)/MWCNT/K mass from 10 to 60 mg was tag along with an increase in MO uptake from 30% to 99.0% [43]. Therefore the dose (40 mg) was the optimum dose and appropriated for all the adsorption studies to verify equilibrium accomplishment. As the quantity of adsorbent raises, the number of active sides obtainable for adsorption also increases thus the removal percentage also increases. But owing to the overlapping between the active sides themselves, not all the obtainable active sides are available during adsorption thus, the amount adsorbed mg/g of adsorbent may be decreased [44].

### 3.6. Effect of agitation speed

Fig. 9 investigates the significance of altering the shaking speed from 50 to 250 rpm on the removal efficiency. The obtained results demonstrate that increasing the shaking rate up to 150 rpm has a positive result on the adsorption of MO onto P(VDF–TrFE)/MWCNT/K nanocomposite. These results could be ascribed to the enhancement in dye dispersion and increase the exposed adsorbent surface area to the dye molecules. Additionally, raising the agitation rate improves the diffusion of dye towards the adsorbent surface. In contrast, a further rise in the agitation velocity up to 200 rpm creates a decline in the adsorption affinity. This declining could be as a result of a further speedup in the agitation rate beyond 200 rpm could diminish the attraction forces between the adsorbent and MO and promote the occurrence of dye desorption process. Thus agitation speed of 200 rpm selected as the optimum speed and appropriated for all the adsorption studies to verify equilibrium accomplishment.

### 3.7. Effect of temperature

The temperature has important effects on the adsorption process. The effect of temperature on the adsorption isotherm of the Methyl orange on P(VDF–TrFE)/MWCNT/K nanocomposite was studied at 298, 305, 308, 313, and 318 K. The results displayed in Fig. 10 revealed that the adsorption capacity decreased from 63.5 to 55.625 mg/g with rising the temperature from 298 to 318 K. This decrease in the adsorption capacity may be attributed to the enhancement of the desorption step in the adsorption mechanism indicating that the process is exothermic. It is well known that the decrease in the amount adsorbed with the increasing the temperature is mainly due to the weakening of sorptive forces between the active sites on the adsorbent and Methyl

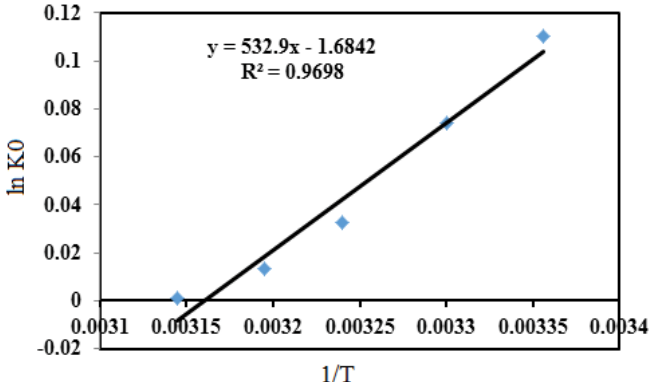


Fig. 10. Variation of $\ln K_0$ vs. $1/T$ for the estimation of thermodynamic parameters.

orange species, and also between adjacent dye molecules on the sorbed phase [45].

Thermodynamic parameters for the adsorption of Methyl orange onto P(VDF–TrFE)/MWCNT/K nanocomposite are given in Table 2. As shown in the table, the negative value of $\Delta G$ ranged from –1.151 to –4.674 kJ/mol confirm the feasibility of the process and spontaneous nature of adsorption. The values of $\Delta H$ and $\Delta S$ are found be (3.87) kJ/mol and (147) J/mol K. respectively.

The positive value of the enthalpy implying that the adsorption process is endothermic and low temperature makes the adsorption easier. The enthalpy value (3.87) is also confirmed that the adsorption is chemisorption as it is larger than that of physisorption. Therefore, the adsorption of the Methyl orange dye under examination onto P(VDF–TrFE)/MWCNT/K nanocomposite is likely due to chemisorption. This result shows that the interaction between the dye and the P(VDF–TrFE)/MWCNT/K nanocomposite is mainly electrostatic interactions [46]. Besides, the positive value of $\Delta S$ suggests randomness at the solid/liquid interface during the adsorption of Methyl orange on nanocomposite in the aqueous solution.

### 3.8. Adsorption isotherms

The linear equations of three of the most customarily applied isotherm models "Langmuir and Freundlich models" were applied in the current study to clarify and interpret the mode of fundamental interaction between MO ions in the solution and the active sites on the P(VDF–TrFE)/MWCNT/K surface (Table 3). The linear plots of these equations are shown in Figs. 11a–b and the computed parameters are represented Table 8.

The maximum monolayer adsorption capacity ($q_{max)}$ was recorded as 62.89 mg/g using the prepared nanocomposite, while [26] conducted that it reached 33.8 mg/g by bentonite, also [47] concluded that $q_{max}$ = 52.86 using MWCNTs but [48] recorded that $q_{max}$ reached 16.78 using activated clay and [49] confirmed that $q_{max}$ reached 41.67 and 34.48 mg/g using organic matter rich clays and calcinated organic matter rich clays respectively. Finally [50] concluded that $q_{max}$ equals 62.5 using modified cafe waste. From the last results the current adsorbent nanocomposite P(VDF–TrFE)/MWCNT/K is the efficient low-cost material.

Table 2
Sorption thermodynamics parameters for MO removal using P(VDF–TrFE)/MWCNT/K

| $\Delta H$ (J/mol) | $\Delta S$ (J/mol K) | $\Delta G$ (kJ/mol) |
|---|---|---|
| 3.87 | 147 | (–1.151) to (–4.674) |

Table 3
Isotherm parameters of the MO adsorption by P(VDF–TrFE)/MWCNT/K nanocomposite

| Adsorption system | Langmuir | | | | Freundlich | | |
|---|---|---|---|---|---|---|---|
| | $q$ (mg/g) | $b$ (L/mg) | $R^2$ | $R_L$ | $K_F$ | $n$ | $R^2$ |
| MO | 62.89 | 0.492 | 0.9973 | 0.0199 | 19.9 | 2.45 | 0.7385 |

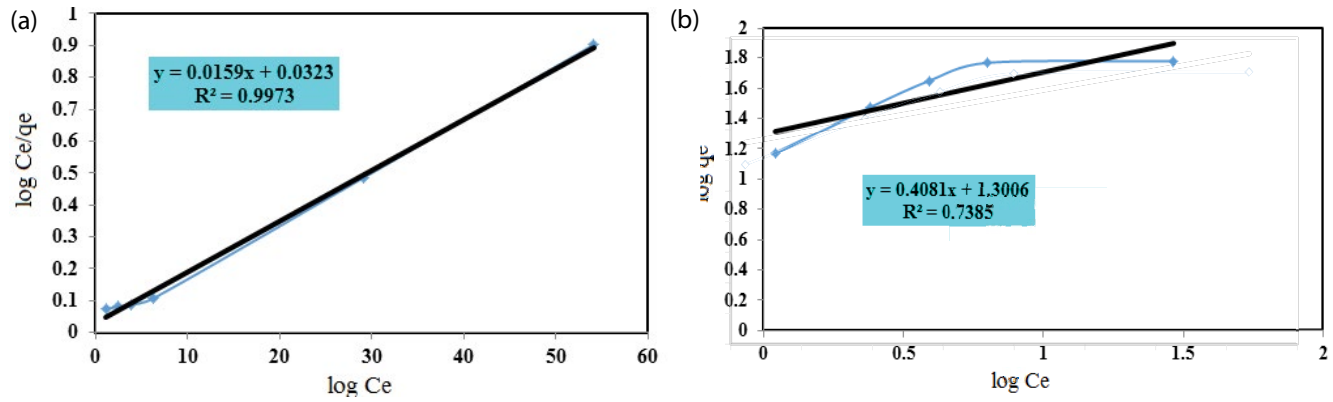


Fig. 11. (a) Langmuir and (b) Freundlich isotherms.

*3.9. Adsorption kinetics*

The kinetics of MO removal by P(VDF–TrFE)/MWCNT/K nanocomposite was studied based on the linear form of the most commonly used models (pseudo-first-order, pseudo-second-order and inter-particle diffusion models). The kinetics of the sorption of MO was studied on the basis of two most commonly used models; pseudo-first-order (Lagergren equation) and pseudo-second-order kinetic model.

Pseudo-first-order:

$$\log\left(q_e - q_t\right) = \log q_e - \left(\frac{K_{ad}}{2.303}\right)t \tag{6}$$

Pseudo-second-order:

$$\frac{t}{q_t} = \frac{1}{k_2 q^2} + \frac{t}{q^2 t} \tag{7}$$

where $q$ (mg/g) is the amount of metal ions sorbed at time $t$, $q_e$ (mg/g) is the amount sorbed at equilibrium and $K_{ad}$ is the equilibrium rate constant of sorption. The straight-line plot shown in Fig. 12a indicates the validity of the equation and the process follows the first-order rate kinetics. The $K_{ad}$ and $q_e$ values of Methyl orange were calculated from the intercept and slope respectively, the results are given in Table 4.

On the other hand, the adsorption rate can be is given by the following equation:

$$h = K_2 q_e^2 \tag{8}$$

where $K_2$ (g/mg min) is the rate constant of the pseudo-second-order (Fig. 12b). The $q_e$ and $K_2$ values can be obtained from the slope and intercept of plots of $t/q_t$ vs. $t$. Values of the related parameters for the adsorption of MO by P(VDF–TrFE)/MWCNT/K have been listed in Table 4. It is seen for the MO in both the kinetic model analysis; the values of the correlation coefficients were found 0.9945 and 0.9179.

The sorption of Methyl orange from aqueous media by the synthesized nanocomposite can be described by three consecutive steps: (i) the transport of sorbate from the bulk solution to the outer surface of the sorbent by molecular diffusion, known as external diffusion, (ii) internal diffusion that is, the transport of sorbate from the particle surface into interior sites, and (iii) the sorption of the solute particles from the active sites into the interior surfaces of the pores. The overall rate of the sorption process will be controlled by the slowest step; that is, the rate-limiting step. The nature of the rate-limiting step in the batch system can be determined from the properties of the solute and sorbent. Rates of sorption are usually measured by determining the change in the concentration of sorbate with sorbent as a function of time. Linearized of the data is obtained by plotting the amount adsorbed per unit weight of adsorbent ($q_e$) vs. $t^{1/2}$, as shown in Fig. 13 by the following equation:

$$q_e = K_p t^{1/2} + C \tag{9}$$

where $K_p$ is the intraparticle diffusion rate constant.

The sorption rates for the intraparticle diffusion, $K_p$ were calculated from the slopes of the linear portions of the respective plots with units of mg/g/min$^{0.5}$ (not the true reaction rate, but relative rates which are useful for comparative purposes). The two plots have the same general features, initial curved portion followed by linear portion and plateau. The initial curve portions are attributed to the boundary layer diffusion effects. While the linear portions are a result of the intraparticle diffusion effects and the plateau is attributed to the equilibrium. An extrapolation of the linear portion of the plots back to the time$^{0.5}$ axis provides intercepts that are proportional to the extent of boundary layer thickness. The larger the intercept, the greater is the boundary layer effect [51].

## 4. Conclusion

Within the outcomes of the present study, the following conclusions are derived: P(VDF–TrFE)/MWCNT/K

Table 4
Adsorption kinetic parameters for MO removal using P(VDF–TrFE)/MWCNT/K

| Pseudo-first-order | | | Pseudo-second-order | | |
|---|---|---|---|---|---|
| $K_1$ (min$^{-1}$) | $q_e$ | $R^2$ | $q_e$ (mg/g) | $K_2$ | $R^2$ |
| 0.0188 | 5.9 | 0.9841 | 70.92 | 0.0009141 | 0.9987 |

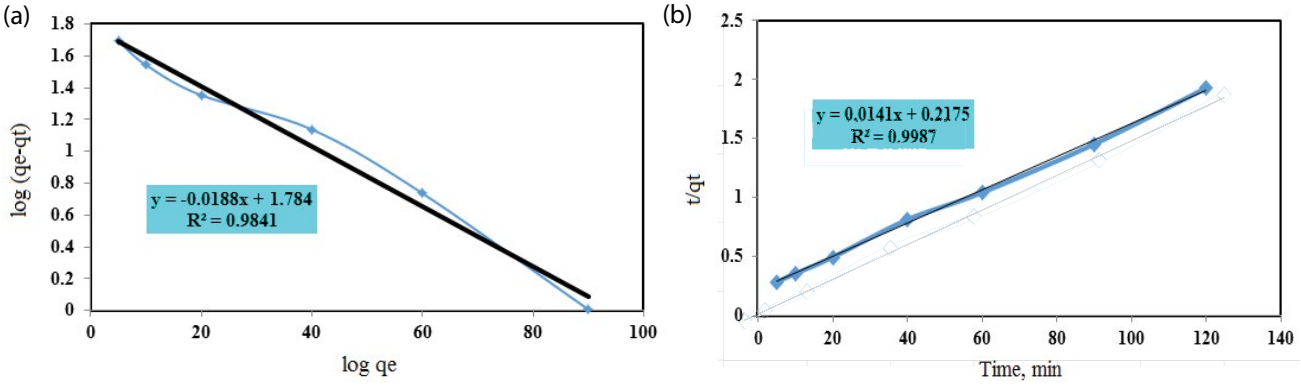


Fig. 12. (a) Pseudo-first-order model and (b) pseudo-second-order model.

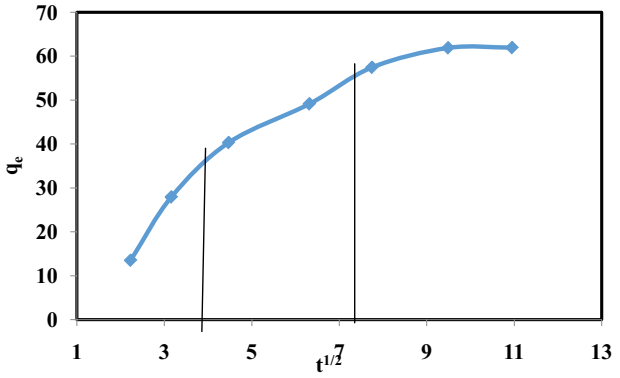


Fig. 13. Intraparticle diffusion model.

nanocomposite is represented as an efficient adsorbent material for the removal of Methyl orange from aqueous solution. Several parameters (time, agitation speed, adsorbent mass, pH, and initial dye concentration) were examined. The results demonstrated that the optimum conditions are (time 90 min, agitation speed 200 rpm, adsorbent mass 40 mg; pH 3, and initial MO concentration is 100 mg/L. Adsorption isotherms indicate that the maximum monolayer coverage is 62.82 mg/g. The adsorption isotherm data fitted well to the Langmuir isotherm ($R^2$ = 0.9984) while the experimental data fitted very well to the pseudo-second-order kinetic model ($R^2$ = 9984). This study suggests that P(VDF–TrFE)/MWCNT/K nanocomposite adsorbent can be used effectively for the adsorption of MO from aqueous solution. The values of $\Delta H$ and $\Delta S$ are found to be 3.87 kJ/mol and (147) J/mole, respectively and the value of $\Delta G$ ranged from –1.151 to –4.674 kJ/mole. At least three times using $H_2SO_4$ (2M) for each regeneration and no loss in the adsorbent mass per cycle. Therefore, P(VDF–TrFE)/MWCNT/K is considered as a better alternative cheap adsorbent for the removal of MO with high efficiency.

## Acknowledgments

The authors gratefully acknowledge Faculty of Earth Sciences, Beni-Suef University, Egypt and Science and technology center of excellence (STCE), National Authority for Military Production, Egypt, as well as Polymer Materials Research Department, Advanced Technology and New Material Institute, City of Scientific Research and Technological Applications (SRTA City) and Faculty of Science, Ain shams University for funding this project.

## References

[1] M. Tuzen, A. Sari, T.A. Saleh, Response surface optimization, kinetic and thermodynamic studies for effective removal of Rhodamine B by magnetic AC/$CeO_2$ nanocomposite, J. Environ. Manage., 206 (2018) 170–177.
[2] S. Kaur, S. Rani, R.K. Mahajan, M. Asif, V.K. Gupta, Synthesis and adsorption properties of mesoporous material for the removal of dye safranin: kinetics, equilibrium, and thermodynamics, J. Ind. Eng. Chem., 22 (2015) 19–27.
[3] W.H. Li, Q.Y. Yue, B.-Y. Gao, Z.-H. Ma, Y.-J. Li, H.-X. Zhao, Preparation, and utilization of sludge-based activated carbon for the adsorption of dyes from aqueous solutions, Chem. Eng. J., 171 (2011) 320–327.
[4] M. Ghaedi, H. Khajesharifi, A. Hemmati Yadkuri, M. Roosta, R. Sahraei, A. Daneshfar, Cadmium hydroxide nanowire loaded on activated carbon as an efficient adsorbent for removal of bromocresol green, Spectrochim. Acta, Part A, 86 (2012) 62–68.
[5] A.M.M. Vargas, A.L. Cazetta, M.H. Kunita, T.L. Silva, V.C. Almeid, Adsorption of Methylene blue on activated carbon produced from flamboyant pods (*Delonix regia*): study of adsorption isotherms and kinetic models, Chem. Eng. J., 168 (2011) 722–730.
[6] A.S. Franca, L.S. Oliveira, M.E. Ferreira, Kinetics and equilibrium studies of Methylene blue adsorption by spent coffee grounds, Desalination, 249 (2009) 267–272.
[7] K.M. Shah, Handbook of Synthetic Dyes and Pigments, 2nd ed., Multitech Publishing Co., India, 1998.
[8] S.A. Abo-El-Enein, M.A. Eissa, A.A. Diafullah, M.A. Rizk, F.M. Mohamed, Removal of some heavy metals ions from wastewater by copolymer of iron and aluminum impregnated with active silica derived from rice husk ash, J. Hazard. Mater., 172 (2009) 574–579.
[9] S.A. Abo-El-Enein, M.A. Eissa, A.A. Diafullah, M.A. Rizk, F.M. Mohamed, Utilization of a low-cost agro-residue for production of coagulant aids and their applications, J. Hazard. Mater., 186 (2011) 1200–1205.
[10] F.M. Mohamed, A.M. kamal, K.A. Alfalous, Recycling of Al(III) from solid waste as alum and alum derivatives and their applications in water and wastewater treatment, Egypt. J. Aquat. Biol. Fish., 23 (2019) 135–146.
[11] N. Mohammadi, H. Khani, V.K. Gupta, E. Amereh, S. Agarwal, Adsorption process of Methyl orange dye onto mesoporous carbon material-kinetic and thermodynamic studies, J. Colloid Interface Sci., 362 (2011) 457–62.
[12] S. Chen, J. Zhang, C.L. Zhang, Q.Y. Yue, Y. Li, Equilibrium and kinetic studies of Methyl orange and Methyl violet adsorption on activated carbon derived from *Phragmites australis*, J. Desal., 252 (2010) 149–156.
[13] T.A. Saleh., V.K. Gupta, Photo-catalyzed degradation of hazardous dye Methyl orange by use of a composite catalyst consisting of multi-walled carbon nanotubes and titanium dioxide, J. Colloid Interface Sci., 371 (2012) 101–106.
[14] Y. Bai, D. Lin, F. Wu, Z. Wang, B. Xing, Adsorption of triton X-series surfactants and its role in stabilizing multi-walled carbon nanotube suspensions, Chemosphere, 79 (2010) 362–367.
[15] L. Ji, Y. Shao, Z. Xu, S. Zheng, D. Zhu, Adsorption of mono aromatic compounds and pharmaceutical antibiotics on carbon nanotubes activated by KOH etching, Environ. Sci. Technol., 44 (2010) 6429–6436.
[16] G.D. Sheng, D.D. Shao, X.M. Ren, X.Q. Wang, J.X. Li, Y.X. Chen, X.K. Wang, Kinetics and thermodynamics of adsorption of ionizable aromatic compounds from aqueous solutions by as-prepared and oxidized multi-walled carbon nanotubes, J. Hazard. Mater., 178 (2010) 505–516.
[17] G.C. Chen, X.Q. Shan, Y.S. Wang, Z.G. Pei, X.E. Shen, B. Wen, G.E. Owens, Effects of copper, lead, and cadmium on the sorption and desorption of atrazine onto and from carbon nanotubes, Environ. Sci. Technol., 42 (2008) 8297–8302.
[18] H. Yan, A. Gong, H. He, S. Zhou, W. Wei, L. Lv, Adsorption of microcystins by carbon nanotubes, Chemosphere, 62 (2006) 142–148.
[19] C. Lu, Y.L. Chung, K.F. Chang, Adsorption of trihalomethanes from water with carbon nanotubes, Water Res., 39 (2005) 1183–1189.
[20] X. Wang, S. Tao, B. Xing, Sorption, and competition of aromatic compounds and humic acid on multi-walled carbon nanotubes, Environ. Sci. Technol., 43 (2009) 6214–6219.
[21] A.A. Elzain, M.R. El-Aassar, F.H. Hashem, F.M. Mohamed, A.S. Ali, Removal of methylene dye using composites of poly (styrene-co-acrylonitrile) nanofibers impregnated with adsorbent materials, J. Mol. Liq., 291 (2019) 111335.
[22] H. Aysan, S. Edebali, C. Ozdemir, M.C. Karakaya, N. Karakaya, Use of chabazite, a naturally abundant zeolite, for the investigation of the adsorption kinetics and mechanism of Methylene blue dye, J. Microporous Mesoporous Mater., 235 (2016) 78–86.

[23] T. Ngulube, J.R. Gumbo, V. Masindi, A. Maity, An update on synthetic dyes adsorption onto clay-based minerals: a state-of-art review, J. Environ. Manage., 191 (2017) 35–57.
[24] G.V. Brião, S.L. Jahn, E.L. Foletto, G.L. Dotto, Highly efficient and reusable mesoporous zeolite synthesized from a biopolymer for cationic dyes adsorption, Colloids Surf., A, 556 (2018) 43–50.
[25] X. An, C. Gao, J. Liao, X. Wu, X. Xie, Synthesis of mesoporous N-doped $TiO_2$/ZnAl-layered double oxides nanocomposite for efficient photodegradation of Methyl orange, Mater. Sci. Semicond. Process., 34 (2015) 162–169.
[26] C. Leodopoulos, D. Doulia, K. Gimouhopoulos, T.M. Triantis, Single and simultaneous adsorption of Methyl orange and humic acid onto bentonite, Appl. Clay Sci., 70 (2012) 84–90.
[27] F.Z. Mahjoubi, A. Khalidi, A. Elhalil, N. Barka, Characteristics and mechanisms of Methyl orange sorption onto Zn/Al layered double hydroxide intercalated by dodecyl sulfate anion, Sci. Afr., 6 (2019) e00216.
[28] M.I. Khan, L. Wu, A.N. Mondal, Z. Yao, L. Ge, T. Xu, Membrane water treatment adsorption of Methyl orange from aqueous solution on anion exchange membranes: adsorption kinetics and equilibrium, 7 (2016) 23–38.
[29] J. Bensalah, A. Habsaoui, B. Abbou, L. Kadiri, I. Lebkiri, A. Lebkiri, E. Rifi, Adsorption of the anionic dye Methyl orange on used artificial zeolites: kinetic study and modeling of experimental data, Mediterr. J. Chem., 9 (2019) 311–316.
[30] D. Ljubas, G. Smoljanic´, H. Juretic, Degradation of Methyl orange and Congo red dyes by using $TiO_2$ nanoparticles activated by the solar and the solar-like radiation, J. Environ. Manage., 161 (2015) 83–91.
[31] F.P. Sejie, M.S. Nadiye –Tabbiruka, Removal of Methyl orange (MO) from water by adsorption onto modified local clay (kaolinite), Phys. Chem., 6 (2016) 39–48.
[32] M. Mobarak, E.A. Mohamed, A.Q. Selim, F.M. Mohamed, L. Sellaoui, A. Bonilla-Petriciolet, M.K. Seliem, Statistical physics modeling and interpretation of Methyl orange adsorption on high–order mesoporous composite of MCM–48 silica with treated rice husk, J. Mol. Liq., 285 (2019) 678–687.
[33] APHA, Standard Methods for Examination of Water and Wastewater, 21st ed., American Public Health Association, Washington, 2005.
[34] S. Langergren, B.K. Svenska, Veternskapsakad, Zur theorie der sogenannten, adsorption geloester stoffe, Handlingar, 24 (1898) 1–39.
[35] L. Langmuir, The constitution and fundamental properties of solids and liquids, J. Am. Chem. Soc., 38 (1916) 2221–2295.
[36] H.M.F. Freundlich, Over the adsorption in solution, J. Phys. Chem., 57 (1906) 385–471.
[37] J.H. van't Hoff, Die Rolle des osmotischen Druckes in der Analogie zwischen Lösungen und Gasen, Z. Phys. Chem., 1 (1887) 481–508.
[38] V. Sencadas, C.M. Costa, V. Moreira, J. Monteiro, S.K. Mendiratta, J.F. Mano, S. Lanceros-Méndez, Poling of β-poly(vinylidene fluoride): dielectric and IR spectroscopy studies, e-Polymers, 5 (2005).
[39] N. Kouklin, M. Tzolov, D. Straus, A. Yin, J.M. Xu, Infrared absorption properties of carbon nanotubes synthesized by chemical vapor deposition, Appl. Phys. Lett., 85 (2004) 4463–4465.
[40] A. Misra, P.K. Tyagi, P. Rai, D.S. Misra, FTIR spectroscopy of multi-walled carbon nanotubes: a simple approach to study the nitrogen doping, J. Nanosci. Nanotechnol., 7 (2007) 1820–1823.
[41] Z. Haddadain, M.A. Shavandi, Z.Z. Abidin, A.F. Razi, M.H. Ismail, Removal of Methyl orange from aqueous solutions using dragon fruit (*Hylocereus undatus*) foliage, Chem. Sci. Trans., 2 (2013) 900–910.
[42] L. Marcal, E.H. de Faria, M. Saltarello, P.S. Calefi, E.J. Nassar, K.J. Ciuffi, Amine-functionalized titanosilicates prepared by the sol–gel process at adsorbent of Azo-dye orange II, Ind. Eng. Chem. Res., 50 (2011) 239–246.
[43] D.T.A. Al-Heetimi, A.H. Dawood, Q.Z. Khalaf, T.A. Himdan, Removal of Methyl orange from aqueous solution by Iraqi bentonite adsorbent, Ibn Al-Haitham J. Pure Appl. Sci., 25 (2017).
[44] M. Sarioglu, A.A. Utay, Removal of Methylene blue by using biosolid, J. Global NEST, 8 (2006) 113–120.
[45] Y.S. Ho, T.H. Chiang, Y.M. Hsueh, Removal of basic dye from aqueous solution using tree fern as a biosorbent, Process Biochem., 40 (2005) 119–124.
[46] M. Al kan, O. Demirbas, S. Çelik Çapas, M. Doğan, Sorption of acid red 57 from aqueous solution onto sepiolite, J. Hazard. Mater., 116 (2004) 135–145.
[47] Y. Yao, H. Bing, X. Feifei, C. Xiaofeng, Equilibrium and kinetic studies of Methyl orange adsorption on multi-walled carbon nanotubes, J. Chem. Eng., 170 (2011) 82–89.
[48] Q. Ma, F. Shen, X. Lu, W. Bao, H. Ma, Studies on the adsorption behavior of Methyl orange from dye wastewater onto activated clay, Desal. Water Treat., 51 (2013) 3700–3709.
[49] A.M. Zayed, M.S.M. Abdel Wahed, E.A. Mohamed, M. Sillanpää, Insights on the role of organic matters of some Egyptian clays in Methyl orange adsorption: isotherm and kinetic studies, Appl. Clay Sci., 166 (2018) 49–60.
[50] R. Lafi, A. Hafiane, Removal of Methyl orange (MO) from aqueous solution using cationic surfactants modified coffee waste (MCWs), J. Taiwan Inst. Chem. Eng., 58 (2016) 424–433.
[51] F. Stoeckli, Porosity in Carbons-Characterization and Applications, J. Patrick ed., Porosity in Carbons, London, Arnold, 1995, pp. 66–97.